

Protonation sites and dissociation mechanisms of *t*-butylcarbamates in tandem mass spectrometric assays for newborn screening

Zdeněk Spáčil, Renjie Hui,[†] Michael H. Gelb* and František Tureček*

Structures of *tert*-butylcarbamate ions in the gas-phase and methanol solution were studied for simple secondary and tertiary carbamates as well as for carbamate-containing products and internal standards for lysosomal enzyme assays used in newborn screening of a α -galactosidase A deficiency (Fabry disease), mucopolysaccharidosis I (Hurler disease), and mucopolysaccharidosis II (Hunter disease). The protonation of simple *t*-butylcarbamates can occur at the carbonyl group, which is the preferred site in the gas phase. Protonation in methanol solution is more favorable if occurring at the carbamate nitrogen atom. The protonation of more complex *t*-butylcarbamates occurs at amide and carbamate carbonyl groups, and the ions are stabilized by intramolecular hydrogen bonding, which is affected by solvation. Tertiary carbamates containing aminophenol amide groups were calculated to have substantially greater gas-phase basicities than secondary carbamates containing coumarin amide groups. The main diagnostically important ion dissociation by elimination of 2-methylpropene (isobutylene, *i*-C₄H₈) and carbon dioxide is shown by experiment and theory to proceed in two steps. Energy-resolved collision-induced dissociation of the Hurler's disease enzymatic product ion, which is a coumarin-diamine linker-*t*-butylcarbamate conjugate (3a⁺), indicated separate energy thresholds for the loss of *i*-C₄H₈ and CO₂. Computational investigation of the potential energy surface along two presumed reaction pathways indicated kinetic preference for the migration of a *t*-butyl hydrogen atom to the carbamate carbonyl resulting in the isobutylene loss. The consequent loss of CO₂ required further proton migrations that had to overcome energy barriers. Copyright © 2011 John Wiley & Sons, Ltd.

Keywords: *t*-butyl carbamates; proton affinities; newborn screening; lysosomal storage disorders; ab initio calculations

INTRODUCTION

The *tert*-butoxycarbonyl (*t*-BOC) group serves as a useful protecting group in peptide and other syntheses that use active ester coupling methods^[1]. *t*-BOC groups are readily removed by a reaction with trifluoroacetic acid, indicating the protonation of the carbamate functionality as the initial cleavage step^[2]. Dissociations of gas-phase cations containing *t*-butylcarbamate groups proceed by a coupled elimination of 2-methylpropene (isobutylene, *i*-C₄H₈) and carbon dioxide to result in the combined loss of 100 Da neutral fragments (Scheme 1)^[3]. The dissociation has been extensively used in tandem mass spectrometry for the quantification of enzyme products and internal standards by multiplex protocols for the detection of lysosomal storage disorders^[4,5] caused by several enzyme deficiencies, for example, acid α -glucosidase (Pompe disease)^[6–8], acid α -galactosidase (GLA, Fabry disease)^[6–8], α -L-iduronidase (mucopolysaccharidosis [MPS] I, Hurler disease)^[9], iduronate-2-sulfatase (MPS-II, Hunter disease)^[10,11], *N*-acetylgalactosamine-6-sulfatase (MPS-IVA, Morquio A disease)^[12], and *N*-acetylgalactosamine-4-sulfatase (MPS VI, Maroteaux-Lamy disease)^[13].

The fragmentation of *t*-BOC-derivatized primary and secondary amines proceeds as a major dissociation pathway in the presence of other groups that are usually considered to be labile, such as α - and β -arylglycosides^[9]. However, the protonation sites in *t*-butylcarbamates and the dissociation mechanisms of pertinent gas-phase cations have not been studied. Carbamic acid, which is the simplest molecule having the carbamate group, prefers protonation at the carbonyl oxygen, as established by both high-level *ab initio* calculations^[14,15] and studies of dissociation mechanisms

after electron transfer^[15]. Gaining insight into the mechanism and energetics of dissociations involving *t*-BOC-containing gas-phase ions is pertinent and requisite for the further development and optimization of tandem mass spectrometric methods to be applied in metabolite analysis. Here we report a joint experimental and computational study that addresses the structures and fragmentation of *t*-butylcarbamate cations relevant to tandem mass spectrometry assays of enzymes used in newborn screening of lysosomal storage disorders.

EXPERIMENTAL

Materials

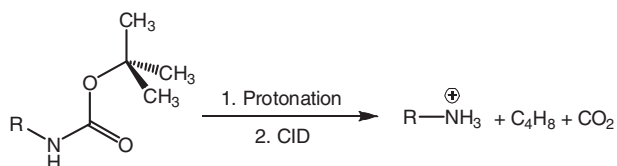
Compounds **3** (internal standard for MPS I assay)^[9], **4** (product of MPS II assay)^[11], and **5** (internal standard for GLA assay)^[6] were synthesized as described previously.

* Correspondence to: Michael H. Gelb, Department of Chemistry, Bagley Hall, Box 351700, University of Washington, Seattle, WA 98195-1700, USA.
E-mail: gelb@chem.washington.edu

* František Tureček, Department of Chemistry, Bagley Hall, Box 351700, University of Washington, Seattle, WA 98195-1700, USA.
E-mail: turecek@chem.washington.edu

Department of Chemistry, Bagley Hall, Box 351700, University of Washington, Seattle, WA, 98195-1700, USA

[†] Current address: DCMR, Ecole Polytechnique, Palaiseau, France.



Scheme 1. Loss of i -C₄H₈ and CO₂ from protonated t -butylcarbamates.

Methods

Mass spectra were measured on the Waters Quattro Micro API bench-top tandem quadrupole mass spectrometer (Waters, Milford, MA). Ions were produced by electrospray ionization from methanol–water–formic acid (50:50:0.1 v/v/v) solutions at concentration of 30 μ M. The experimental parameters were as follows: flow rate, 5 μ l/min; needle voltage, 3500 V; drying gas temperature, 200 °C; flow rate, 200 l/h; and cone voltage, 5.25 V. Argon was used as a collision gas at nominal pressures that were varied between 1.3×10^{-4} and 5.2×10^{-4} Torr. Selected ion monitoring of m/z 377, 321, and 277 ions was performed while the acceleration voltage was ramped in 1 V steps from 0 to 20 V corresponding to nominal ion laboratory kinetic energies in the same electron volt range.

Calculations

Standard *ab initio* and density functional theory calculations were performed using the Gaussian 09 suite of programs [16]. Gas-phase structures were optimized with B3LYP/6-31+G(d,p) [17], and the local energy minima and transition states were confirmed by frequency calculations as having the appropriate number of imaginary frequencies (0 for minima, 1 for saddle points). All relative energies were corrected for zero-point vibrational energies based on harmonic frequencies that were scaled by 0.963 [18]. Transition states were located by scanning with B3LYP/6-31+G(d,p) the potential energy surface between the reactant and the product. Intermediate structures of low energy gradients along the reaction coordinate X ($dE/dX < 0.005$) were analyzed by harmonic frequency calculations, and the calculated Hessian matrix was used for saddle point search and optimization.

Single-point energies on fully optimized geometries were calculated with B3LYP/6-311++G(2d,p) and MP2/6-311++G(2d,p) [19] and averaged to cancel out known errors in each method [20]. Benchmark single-point energies were calculated using coupled clusters [21] with single, double, and disconnected triple excitations, CCSD(T) [22], and the 6-311G(d,p) basis set and expanded to effective CCSD(T)/6-311++G(3df,2p) using the standard linear formula: $E[\text{CCSD(T)/6-311++G(3df,2p)}] \approx E[\text{CCSD(T)/6-311G(d,p)}] + E[\text{MP2/6-311++G(3df,2p)}] - E[\text{MP2/6-311G(d,p)}]$ [23]. Calculations of solvated ions used the polarizable continuum model (PCM) [24] with standard parameters for methanol included in Gaussian 09. Solvated ion structures were fully optimized with PCM-B3LYP/6-31+G(d,p) using the pertinent gas-phase ion structures as initial guesses. Frequency calculations of solvated ions were not performed. Enthalpies and entropies were obtained from standard thermodynamic formulas using the rigid-rotor-harmonic oscillator model for the vibrational and rotational terms. Vibrational enthalpy terms for very low frequencies that exceeded 0.5 kT were replaced by the 0.5-kT term for free rotations [25]. Vibrational entropies were not corrected. Proton affinities and gas-phase basicities were calculated as the respective 298 K reaction enthalpies and free energies for a dissociation of ion AH⁺ to neutral molecule A and a proton. Unimolecular rate constants were calculated using the Rice–Ramsperger–Kassel–Marcus (RRKM) theory [26] and using a modified Hase's program [27], which was recompiled for Windows XP [28] and Windows 7. The RRKM rate constants were obtained by direct count of quantum states at internal energies that were increased in 2 kJ mol⁻¹ steps from the transition state up to 400 kJ mol⁻¹ above the reactant. Rotations were treated adiabatically, and the calculated microscopic rate constants $k(E,J,K)$ were then Boltzmann-averaged over the thermal distribution of rotational states at 298 K.

RESULTS AND DISCUSSION

We addressed five structure types containing the t -butylcarbamate group. The chemical structures of the representative neutral compounds are shown in Fig. 1. Structures **1** and **2** are simple N -methyl and N,N -dimethyl t -butylcarbamates that were used as basic

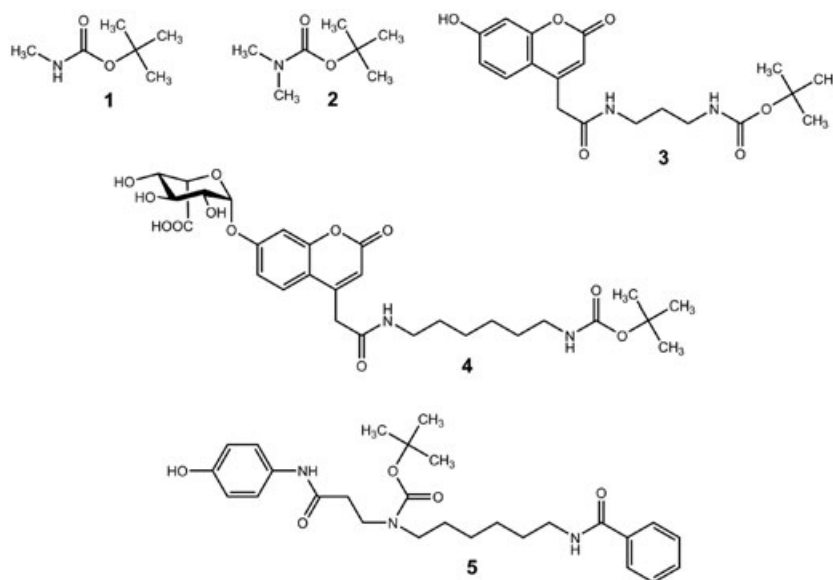


Figure 1. Chemical structures of neutral t -butylcarbamates.

representatives of the functional groups of interest. Protonation in these systems is not affected by hydrogen bonding or interactions with other functional groups in the ion and thus represents the intrinsic property of the *t*-butylcarbamate moiety. Structure **3** represents the internal standard for the MPS-I assay. The molecule has a 7-hydroxycoumarin ring, which is conjugated to a diamine linker capped with a *t*-BOC group. Structure **4** is the enzymatic product of the MPS-II assay, which is an α -glycoside of α -L-iduronic acid and a coumarin conjugate aglycon. Structure **5** is the product of the GLA assay, which is chemically identical to the deuterium-labeled GLA internal standard^[6], both consisting of an aminophenol, a 1,6-hexanediamine linker with a tertiary *t*-BOC group, and a benzamide. The common feature of structures **3–5** is that they contain several potential protonation sites in the aromatic rings, amide groups, and the carbamate group.

Energy-resolved collision-induced dissociations

We first present experimental results from energy-resolved CID of ion **3**⁺ formed by electrospray protonation of **3**. Figure 2 shows the breakdown diagrams for the *m/z* 377 precursor ion of **3**⁺, the *m/z* 321 product ion by elimination of C₄H₈, and the *m/z* 277 product ion due to a combined elimination of C₄H₈ and CO₂, which are plotted against the center-of-mass collision energy (E_{CM}). The breakdown diagrams were measured at three different nominal collision gas pressures; shown are the curves for the highest 5.2×10^{-4} Torr and lowest 1.3×10^{-4} Torr pressures. The curves obtained at the lowest pressure indicate a dissociation onset at ca. $E_{\text{CM}} = 0.5$ eV for 1% elimination of C₄H₈ in the *m/z* 321 channel. The onset for the *m/z* 277 ion is shifted

by 0.2–0.3 eV to higher E_{CM} . Note that these energies have not been extrapolated to single-collision conditions and must be viewed as lower bounds for the real threshold energies^[30]. However, the fact that there are two separate onsets indicates that the formation of the *m/z* 277 ion occurs by *consecutive losses* of C₄H₈ and CO₂, whereby the *m/z* 321 fragment ion is a stable intermediate that requires additional excitation to eliminate CO₂. The relatively small difference in the estimated onset energies does not allow us to unequivocally exclude the presence of an alternative, presumably minor, pathway, which is a concomitant elimination of C₄H₈ and CO₂ through a short-lived intermediate. Obviously, such an elimination would have a different mechanism from that forming the stable *m/z* 321 intermediate. Adding the estimated threshold energy for the elimination of C₄H₈ (0.5 eV) to the thermal energy (E_{th}) of the precursor ion gives a rough estimate of the critical energy (E_{T5}) for the dissociation. Because the precursor ions entering the collision cell may not be at thermal equilibrium, their temperature and internal energy can vary from ambient ($E_{\text{th}} = 0.58$ eV at 298 K) to that of the electrospray interface ($E_{\text{th}} = 1.36$ eV at 473 K). This gives a broad range of the estimated $E_{\text{T5}} \approx 0.5 + E_{\text{th}} = 1.08 \sim 1.86$ eV = 104–180 kJ mol⁻¹.

Protonation of simple *t*-butylcarbamates

The fragmentation of protonated carbamates raises questions regarding the structures and energies of the precursor ions, transition states, and intermediates as well as the overall dissociation energies for the eliminations of C₄H₈ and CO₂. The protonation of the carbamate group in simple *t*-butylcarbamates can in principle take place at one of the oxygen atoms or at the nitrogen atom. Protonated **1** (Fig. 3) shows the carbonyl (**1a**⁺) and *N*-protonated ion structures (**1b**⁺) as the most stable tautomers. Ion **1a**⁺ is calculated to be 20 kJ mol⁻¹ more stable than **1b**⁺ in the gas phase, indicating a higher proton affinity for the carbonyl oxygen in the secondary carbamate (Table 1). This preference is greatly diminished or even reversed in a methanol solution where the solvated ions **1a**⁺ and **1b**⁺ are practically isoenergetic. Our highest-level calculations at the effective CCSD(T)/6-311++G(3df,2p) level of theory give $\Delta G^{\circ}_{298}(\mathbf{1a}^+ \rightarrow \mathbf{1b}^+) = 18$ and -3 kJ mol⁻¹ in the gas-phase and methanol solution, respectively. The ether-protonated tautomer (**1c**⁺) was substantially less stable than **1a**⁺ and **1b**⁺ in both the solution and the gas phase. The methanol-solvated structure of **1c**⁺ has long C—O bonds (Fig. 3), indicating partial dissociation to a solvated complex of *N*-methylcarbamic acid and *t*-butyl cation, which is again less stable than solvated **1a**⁺ and **1b**⁺.

Additional *N*-methylation in **2** increases the overall carbamate gas-phase basicity (GB) by 21 kJ mol⁻¹ (Table 1). A particular increase is seen for the nitrogen atom, which is comparably basic as the carbonyl oxygen. The *N*-protonated tautomer (**2b**⁺; Fig. 3) is only marginally less stable than the carbonyl protonated structure **2a**⁺ in the gas phase. The stability order is reversed in methanol solution where solvated **2b**⁺ is more stable than **2a**⁺. The calculated energies indicate that simple *t*-butylcarbamates slightly prefer to be protonated at the nitrogen atom in methanol solution, but not in the gas phase. Considering that protonation in electrospray takes place in liquid droplets, the initially formed ions should consist of mixtures of *O*-carbonyl and *N*-protonated tautomers, with the latter being favored. However, as the gas-phase ions travel into the mass spectrometer, they can exchange

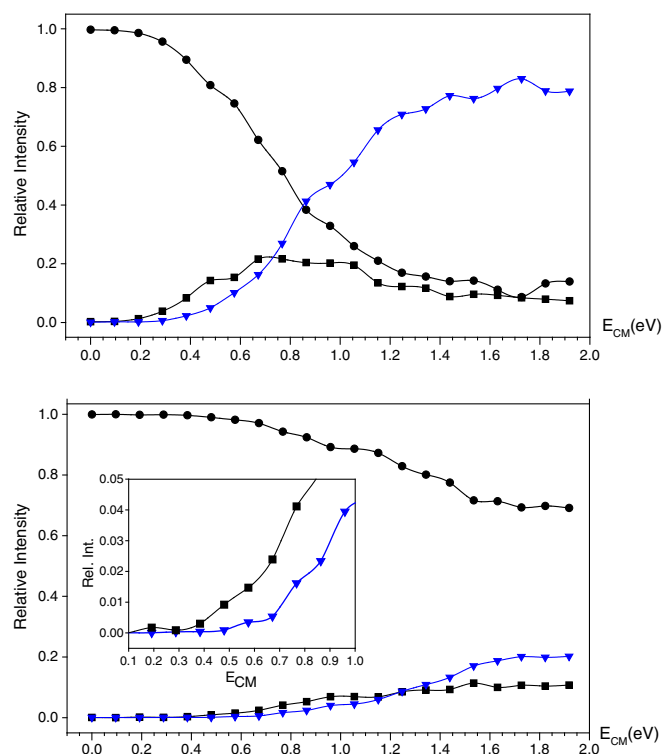


Figure 2. Energy-resolved collision-induced dissociation of **3**⁺ at nominal collision gas pressures of (top) 5.2×10^{-4} and (bottom) 1.3×10^{-4} Torr. Black circles: *m/z* 377; black squares: *m/z* 321; blue triangles: *m/z* 277. Inset shows the enlarged section of fragment ion relative intensities between 0.1 and 1.0 eV.

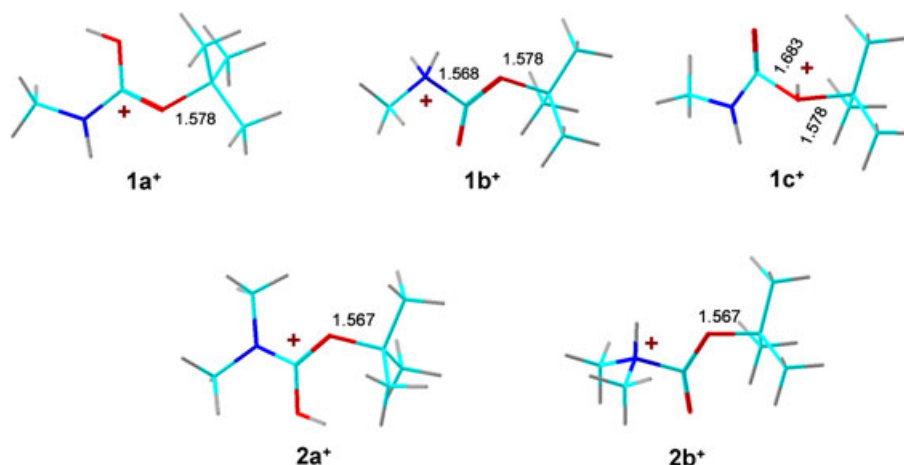


Figure 3. B3LYP/6-31 + G(d,p)-optimized structures of ion tautomers of 1^+ and 2^+ . The atoms are color coded as follows: green = C; red = O; blue = N; gray = H.

Table 1. Ion-relative energies

Species/reaction	Relative energy ^{a,b}				
	B3LYP 6-31+G(d,p)	B3LYP 6-311++G(2d,p)	MP2	B3-MP2 ^c 6-311++G(2d,p)	CCSD(T) ^d 6-311++G(3df,2p)
$1a^+ \rightarrow 1 + H^+$	882	883	865	874 (879) ^e	877 (882) ^e (850) ^f
$1a^+ \rightarrow 1b^+$	27	25	12	18 (17) ^g (-4) ^h	20 (18) ^g (-3) ^h
$1a^+ \rightarrow 1c^+$	81	79	76	77 (72) ^g (45) ^h	
$2a^+ \rightarrow 2 + H^+$	898	899	884	892 (899) ^e	896 (903) ^e (871) ^f
$2a^+ \rightarrow 2b^+$	14	13	1	7 (9) ^g (-10) ^h	6 (8) ^g (-11) ^h
$3a \rightarrow 3b$	1	0.5	15	8 (1.5) ^g	
$3a^+ \rightarrow 3a + H^+$	966	966	943	954 (961) ^e (924) ^f	
$3a^+ \rightarrow 3b^+$	22	22	31	26 (23) ^g (48) ^h	
$3a^+ \rightarrow 3c^+$	41	39	26	33 (29) ^g (18) ^h	
$3a^+ \rightarrow 3d^+$	79	78	66	72 (71) ^g (63) ^h	
$4a \rightarrow 4b$	12	13	-13	0 (9) ^g	
$4a^+ \rightarrow 4a + H^+$	960	958	967	962 (970) ^e (918) ^f	
$4a^+ \rightarrow 4b^+$	17	16	55	35 (21) ^d (31) ^h	
$5a \rightarrow 5b$	-1	-1	-1	-1 (-1) ^g	
$5a^+ \rightarrow 5a + H^+$	992	990	998	994 (1001) ^e (950) ^f	
$5a^+ \rightarrow 5b^+$	4	1	37	19 (3) ^g (-39) ^h	
$5a^+ \rightarrow 5c^+$	17	17	12	14 (10) ^g (-1) ^h	
$5a^+ \rightarrow 5d^+$	50	45	64	55 (36) ^g (-13) ^h	
$5a^+ \rightarrow 5e^+$	80	77	101	89 (71) ^g (-11) ^h	

^aIn units of kJ mol^{-1} .

^bIncluding B3LYP/6-31 + G(d,p) zero-point energies and referring to 0K unless stated otherwise.

^cFrom averaged B3LYP and MP2 single-point energies.

^dFrom effective single-point energies.

^eProton affinities at 298 K.

^fGas-phase basicities at 298 K.

^gRelative gas-phase free energies at 298 K.

^hRelative free energies in methanol solution at 298 K.

protons with the residual neutral carbamate molecules to preferentially form O-carbonyl protonated tautomers. The actual composition of the gas-phase ion tautomer population then may depend on the experimental conditions that determine the interactions in the solution and in the gas phase. The energy data in Table 1 further show that the relatively inexpensive B3-MP2/6-311++G(2d,p) calculations gave excellent results for the ion

energetics when benchmarked against the effective CCSD(T)/6-311++G(3df,2p) data. The B3-MP2 scheme was therefore used for calculations of the larger MPS-I, MPS-II, and GLA molecules and ions. These systems include several functional groups, providing multiple protonation sites and ion stabilization by intramolecular hydrogen bonding. Ion structures for these three groups are presented in the next section.

Protonation of coumarin and aminophenol conjugates

Geometry optimization of the MPS-I internal standard **3** produced two structures that differed in the conformation of the diamine linker. Structure **3a** had the carbamate NH hydrogen bonded to

the amide carbonyl (Fig. 4). Structure **3b** had an extended linker. The calculated gas-phase free energies slightly favor **3a** by 1.5 kJ mol^{-1} at 298 K. This order of relative free energies is reversed at temperatures $>360 \text{ K}$ because of the higher entropy of the extended-chain conformer **3b**. Protonation in **3a** or **3b** can occur in

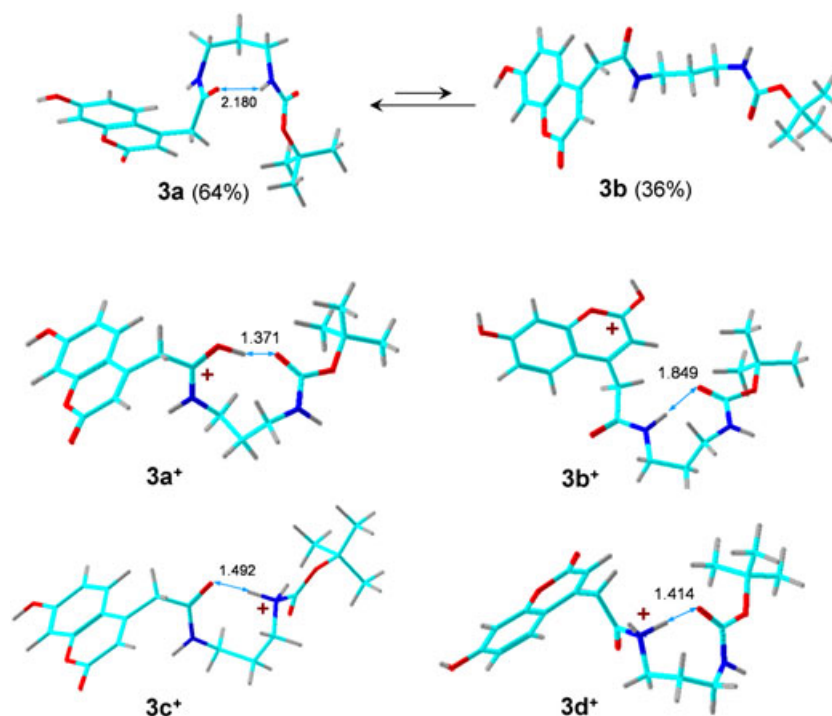


Figure 4. B3LYP/6-31 + G(d,p)-optimized structures of ion tautomers of 3^+ . The atoms are color coded as follows: green = C; red = O; blue = N; gray = H.

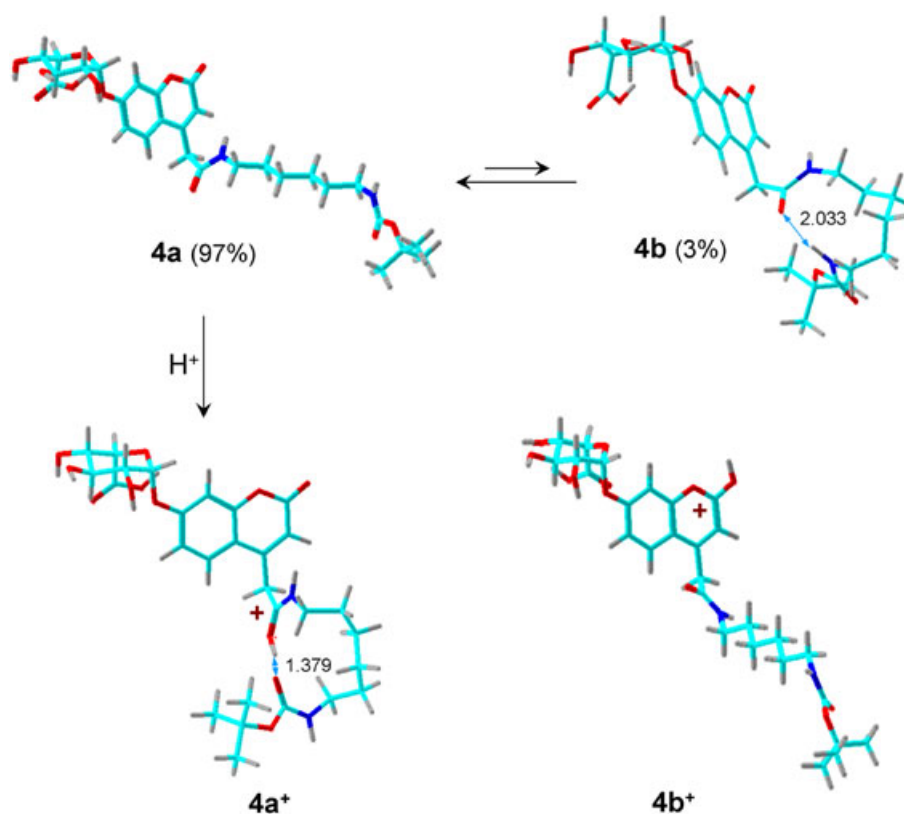


Figure 5. B3LYP/6-31 + G(d,p)-optimized structures of ion tautomers of 4^+ . The atoms are color coded as follows: green = C; red = O; blue = N; gray = H.

several positions, leading to tautomers $3a^+$ – $3d^+$ (Fig. 4). The amide carbonyl-protonated tautomer $3a^+$ was calculated to be the most stable cation in both the gas-phase and the methanol solution (Table 1), followed by the coumarin-protonated tautomer $3b^+$.

Protonation at the amide and carbamate nitrogen atoms leads to high-energy tautomers. Interestingly, an ion tautomer protonated at the carbamate carbonyl was not a local energy minimum and upon optimization spontaneously isomerized to $3a^+$. Hence,

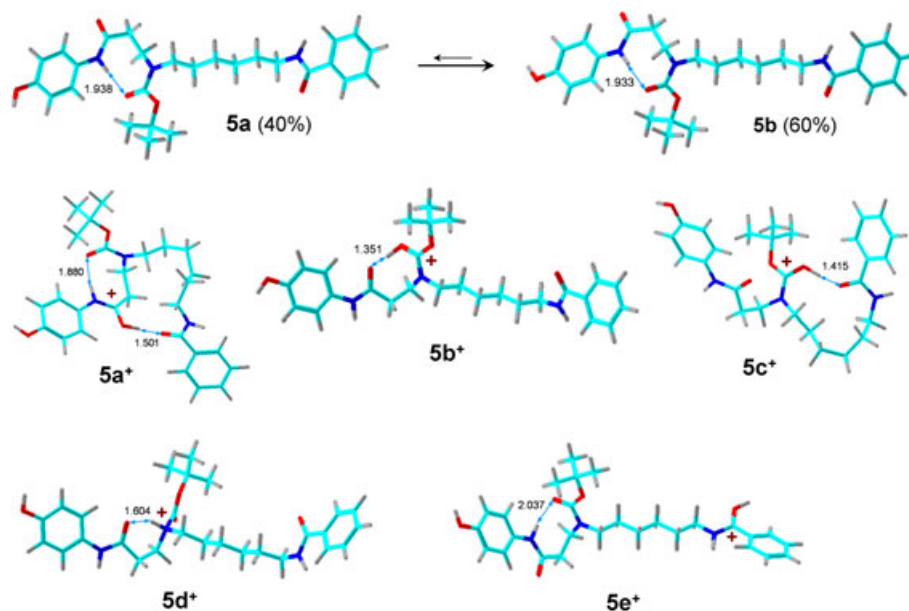


Figure 6. B3LYP/6-31 + G(d,p)-optimized structures of ion tautomers of 5^+ . The atoms are color coded as follows: green = C; red = O; blue = N; gray = H.

Table 2. Ion dissociation and transition state energies

Reaction	Relative energy ^{a,b}			
	B3LYP 6-31+G(d,p)	B3LYP 6-311++G(2d,p)	MP2	B3-MP2 ^c 6-311++G(2d,p)
$3a^+ \rightarrow 3aa^+$	118	106	118	112
$3a^+ \rightarrow \text{TS1}$	141	133	157	145
$3a^+ \rightarrow 3ab^+ + i\text{-C}_4\text{H}_8$	144	130	154	142
$3ab^+ \rightarrow 3ac^+$	-27	-23	-23	-23
$3ab^+ \rightarrow 3ad^+$	-36	-33	-28	-31
$3ab^+ \rightarrow 3ae^+$	-85	-82	-67	-74
$3a^+ \rightarrow 3ae^+ + i\text{-C}_4\text{H}_8$	59	48	87	68
$3a^+ \rightarrow \text{TS2}$	118	103	122	112
$3a^+ \rightarrow 3af^+ + i\text{-C}_4\text{H}_8$	21	2	26	14
$3a^+ \rightarrow 3ag^+ + i\text{-C}_4\text{H}_8 + \text{CO}_2$	40	19	49	34
$3a^+ \rightarrow \text{TS3}$	100	97	124	110
$3a^+ \rightarrow 3ba^+$	83	74	93	84
$3a^+ \rightarrow 3bb^+ + i\text{-C}_4\text{H}_8$	117	107	143	125
$3a^+ \rightarrow \text{TS4}$	128	118	146	132
$3a^+ \rightarrow 3bc^+$	27	18	47	33
$3bc^+ \rightarrow 3ae^+ + i\text{-C}_4\text{H}_8$	31	30	41	35
$3ae^+ \rightarrow \text{TS5}$	53	54	39	46
$3ae^+ \rightarrow 3bc^+$	58	59	44	51
$3ae^+ \rightarrow \text{TS6}$	103	99	88	93
$3ae^+ \rightarrow 3ag^+ + \text{CO}_2$	-18	-29	-39	-34
$3af^+ \rightarrow 3ag^+ + \text{CO}_2$	19	17	23	20

^aIn units of kJ mol^{-1} .

^bIncluding B3LYP/6-31 + G(d,p) zero-point energies and referring to 0 K.

^cFrom averaged B3LYP and MP2 single point energies.

structure **3a⁺** is expected to predominate in the gas-phase ion population. The proton affinity of **3a** forming **3a⁺** was calculated by B3-MP2/6-311++G(2d,p) as PA = 961 kJ mol⁻¹.

Geometry optimization of the glycoside MPS-II product **4** yielded two conformers (**4a** and **4b**; Fig. 5). The extended conformer **4a** was 9 kJ mol⁻¹ more stable ($\Delta G_{g,298}^\circ$) and is expected to predominate in the gas phase. The lower $\Delta G_{g,298}^\circ$ of **4a** is mainly due to its higher entropy compared with that of **4b** as the formation of the 11-membered ring in the latter conformer resulted in a 30-J mol⁻¹ K⁻¹ entropy decrease at 298 K. The protonation of **4a** gave ion **4a⁺** in which the protonated amide group was H-bonded to the carbamate carbonyl (Fig. 5). Protonation at the carbamate carbonyl resulted in an unstable ion structure that upon gradient optimization collapsed to a conformer of **4a⁺**. Protonation at the coumarin carbonyl gave tautomer **4b⁺**, which was less stable than **4a⁺**. In view of the relative stabilities of **3a⁺**–**3d⁺**, we presumed that **4a⁺** was the most stable ion structure and other tautomers were not studied. Table 1 shows that the proton affinity of **4a** (PA = 970 kJ mol⁻¹) was slightly higher than that of **3a**. However, the entropy loss upon formation of the 13-membered H-bonding ring in **4a⁺** lowered the GB of **4a** (918 kJ mol⁻¹) below that of **3a** (924 kJ mol⁻¹).

The optimized structures of the GLA product show an intramolecular H bond between the carbamate carbonyl and the aminophenol N—H bond. The phenol OH group rotamers **5a** and **5b** were nearly isoenergetic. The protonation of **5a/5b** was studied for several ion tautomers (**5a⁺**–**5e⁺**). The lowest-energy ion structure was protonated at the aminophenol amide carbonyl, which was H-bonded to the benzamide carbonyl (**5a⁺**; Fig. 6). The second most stable structure (**5b⁺**) was protonated at the carbamate carbonyl, which was tightly H-bonded to the aminophenol amide (Fig. 6). Attempts to move the proton in **5b⁺** to the aminophenol amide carbonyl resulted in spontaneous collapse back to structure **5b⁺**, indicating that the tertiary carbamate group was more basic. Structures **5a⁺** and **5b⁺** were very close in energy; **5a⁺** was preferred by MP2 calculations, whereas **5b⁺** was preferred by B3LYP calculations. Ion **5b⁺** was slightly more stable than its conformer **5c⁺**, which had an H-bond between the protonated carbamate carbonyl and the benzamide group. Both **5a⁺** and **5b⁺** were substantially more stable than the *N*-protonated structure **5d⁺**. We note that a definite assignment of the global energy minimum for this group of ions would require an exhaustive conformational search for each tautomer, which we have not performed.

The GB of the tertiary carbamate **5a** (950 kJ mol⁻¹) is notably higher than those of the secondary carbamates **3a** and **4a**. The relatively high basicity of the amide group in **5a** is presumably due to π -conjugation with the electron-rich aminophenol system that stabilizes the cation. This is consistent with an experimental observation that the protonation of **5** in electrospray is notably more efficient than the protonation of coumarin conjugates and results in lower limits of detection for the enzyme products and their related internal standards [8].

Dissociation mechanisms for the elimination of isobutylene and carbon dioxide

The elimination of isobutylene was studied for the coumarin-derived ion **3a⁺**. The elimination must involve cleavage of the *t*-butyl C—O bond with a transfer of one of the *t*-butyl hydrogen atoms onto the product ion. The hydrogen acceptor groups and the timing of

the bond cleavage and proton migration were *a priori* unknown and were investigated by mapping the potential energy surface along two pathways. The pertinent relative energies are listed in Table 2 and arrayed in the potential energy diagram (Fig. 7a). Pathway A (Scheme 2) commenced with *t*-butyl hydrogen atom transfer onto the carbamate nitrogen through TS1 in which the *t*-butyl C—O bond was practically completely broken at $d(\text{C—O}) = 3.121 \text{ \AA}$. Concomitantly, a proton from the coumarin amide group migrated to the carbamate moiety to reform the COOH group. The migration required a TS energy of 145 kJ mol⁻¹ (Table 2). The intermediate in this pathway was an ion–molecule complex between an *N*-protonated carbamic acid and a neutral isobutylene (**3aa⁺**), which was 112 kJ mol⁻¹ above **3a⁺**. The direct elimination of *i*-C₄H₈ from **3aa⁺** leads to a high-energy tautomer of the *m/z* 321 ion, which is the *N*-protonated carbamic acid **3ab⁺**. The loss of *i*-C₄H₈ from **3aa⁺** was presumed to occur at the thermochemical threshold, which was 142 kJ mol⁻¹ relative to **3a⁺** (Table 2).

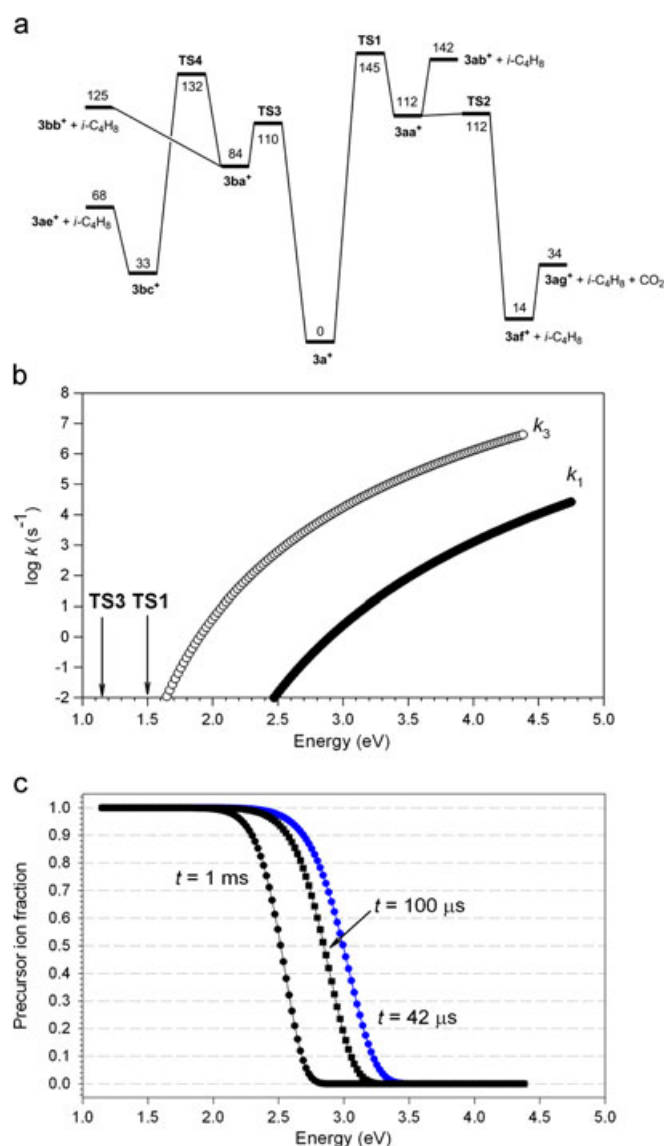
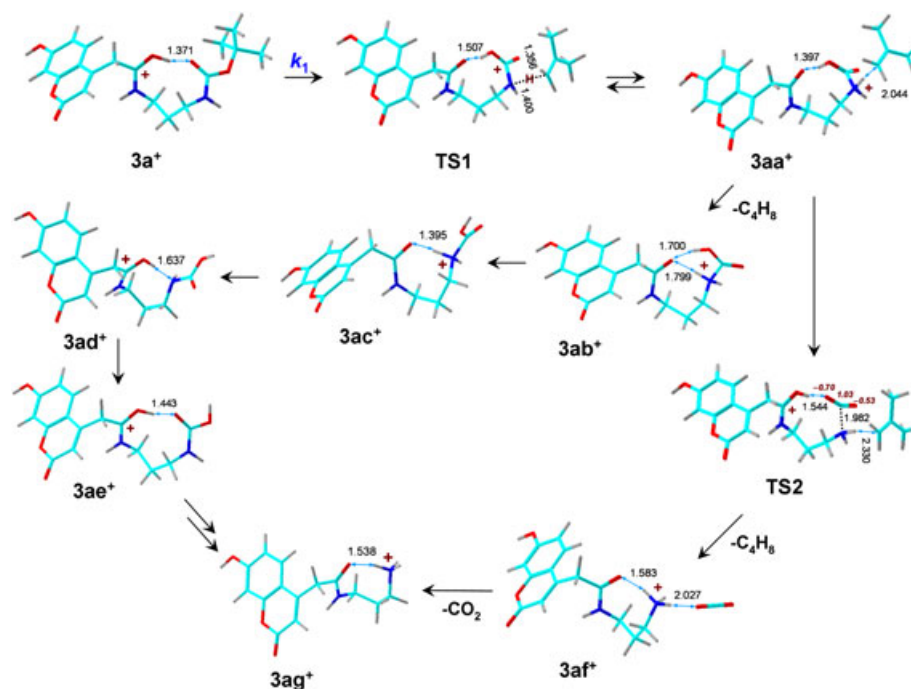


Figure 7. (a) B3-MP2/6-311++G(2d,p) potential energy surface for dissociations of **3a⁺** and (b and c) RRM kinetics of elimination of *i*-C₄H₈. (b) Rate constants for elimination through TS1 (k_1) and TS3 (k_3); (c) calculated fractions of nondissociating **3a⁺** at the indicated reaction times: black circles: 1 ms; black squares: 100 μs ; blue circles: 42 μs .



Scheme 2. Pathway A for dissociations of ion $3a^+$. The atoms are color coded as follows: green = C; red = O; blue = N; gray = H.

If formed, $3ab^+$ can be expected to isomerize by exothermic proton migrations and chain rotations to more stable ions $3ac^+$, $3ad^+$, and $3ae^+$ (Table 2).

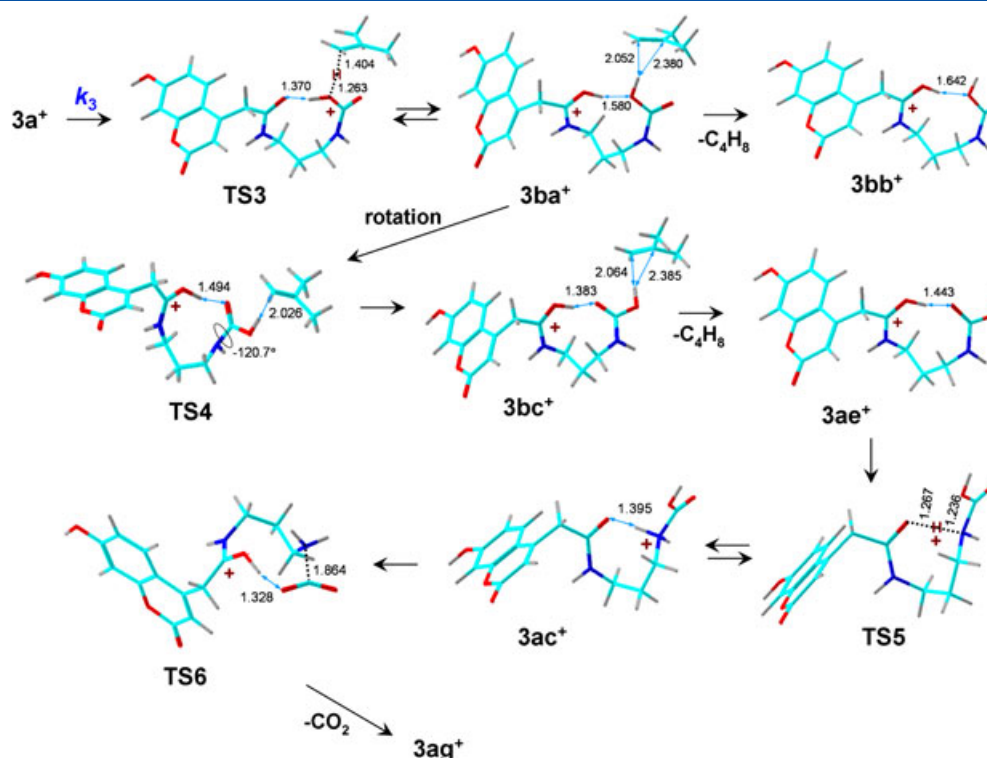
An alternative branch of pathway A from $3aa^+$ was considered, which involved carbamate proton migration to the amide carbonyl in the ion–molecule complex, accompanied by cleavage of the carbamate N–CO₂ bond through TS2, which was practically isoenergetic with $3aa^+$ (Scheme 2). The resulting ion–molecule complex ($3af^+$) contained a weakly bound CO₂ molecule, which required only 20 kJ mol⁻¹ to be eliminated to give the m/z 277 product ion ($3ag^+$). The fact that intermediates $3aa^+$ and TS2 have nearly identical energies, which are lower than that of TS1 (Table 2), suggests that the isobutylene elimination step, $3aa^+ \rightarrow TS2 \rightarrow 3af^+$, should be followed by fast elimination of CO₂ from complex $3af^+$, which does not involve a high TS energy. These features would have a large effect on the dissociation kinetics, as discussed later.

Pathway B involves an initial transfer of a *t*-butyl H atom to the carbamate oxygen atom (Scheme 3). The pertinent TS (TS3) showed a nearly complete cleavage of the *t*-butyl C–O bond and led to an ion–molecule complex ($3ba^+$), which was 84 kJ mol⁻¹ above $3a^+$ (Table 2). The elimination of *i*-C₄H₈ from complex $3ba^+$ can occur endothermically to form ion $3bb^+$ at 125 kJ mol⁻¹ above $3a^+$. An alternative branch involves the rotation of the carbamate COOH group through TS4 ($E_{TS4} = 132$ kJ mol⁻¹ relative to $3a^+$) to give intermediate $3bc^+$, which then loses *i*-C₄H₈ to form the m/z 321 ion as structure $3ae^+$, which is 57 kJ mol⁻¹ lower energy than $3bb^+$. The elimination of CO₂ from both $3ae^+$ and $3bb^+$ must involve proton migration. One possible branch of pathway B proceeds through TS5 to transfer the amide proton onto the carbamate nitrogen and weaken the N–CO₂ bond in intermediate $3ac^+$, which is 51 kJ mol⁻¹ above $3ae^+$. Ion $3ac^+$ reacts by transferring the carbamate COOH proton onto the amide carbonyl with concomitant cleavage of the N–CO₂ bond in TS6, which is 95 kJ mol⁻¹ above $3ae^+$ and represents the highest energy point in the entire pathway B.

Pathways A and B differ in the initial step of *t*-butyl hydrogen migration, which forms isomeric intermediates $3aa^+$ and $3ba^+$ through TS1 and TS3, respectively. These are the high points on the potential energy surface for the elimination of *i*-C₄H₈. We used RRKM calculations to investigate the unimolecular kinetics for loss of *i*-C₄H₈ through TS1 and TS3, as shown in Figs 7b and 7c. The pathway B dissociation was three or more orders of magnitude faster than the pathway A dissociation in the entire energy interval, and both showed substantial kinetic shifts (Fig. 7b). The ion dissociation time scale was limited by the ion drift time through the collision cell, which was estimated to be 75 μs for m/z 377 ions at $E_{LAB} = 5$ eV. A broader range of up to 1 ms was considered in the calculations to account for loss of kinetic energy. Under the conditions of the 1-ms dissociation time, the precursor ion showed no substantial (>1%) depletion up to approximately 2.07 eV internal energy even when the dissociation proceeded through the kinetically more favorable pathway B (Fig. 7c). The RRKM dissociation onset taken at 1% dissociation (2.07 eV) is still higher than the upper energy estimate from the CID experiments (1.86 eV, vide supra). This indicates that the CID measurements involved multiple collisions that increased the ion internal energy to 2.07 eV needed for 1% dissociation to be observed on a 1-ms time scale. The consequent elimination of CO₂ from the m/z 321 intermediate should occur spontaneously if proceeding through pathway A. This is incompatible with the observation of two separate dissociation onsets for the elimination of *i*-C₄H₈ and CO₂. The calculated TS for the loss of CO₂ (95 kJ mol⁻¹ in TS6 from $3ae^+$; Table 2) indicates that additional internal energy is required in the precursor ion to drive the two-step dissociation.

CONCLUSIONS

Protonation and dissociations of three *t*-butyl carbamates that are used in newborn screening of lysosomal storage disorders



Scheme 3. Pathway B for dissociations of ion $3a^+$. The atoms are color coded as follows: green = C; red = O; blue = N; gray = H.

were investigated by experiment and theory. *t*-Butyl carbamates containing aminophenol amide and tertiary carbamate groups (**5**) were calculated to have greater gas-phase basicities than compounds containing a coumarin amide and secondary carbamate groups (**3** and **4**). This was consistent with the higher ionization efficiencies in electrospray observed for the first group of compounds. The favorable protonation sites in types **3** and **4** compounds were at the coumarin amide oxygen in both the gas-phase and the methanol solution. In contrast, the favorable protonation sites in type **5** compounds differed in the gas-phase and methanol solution. Collision-induced dissociation of type **3** ions showed a sequential dissociation by loss of *i*-C₄H₈ and CO₂. Computational investigation of reaction pathways identified several transition states and intermediates and allowed us to propose a plausible mechanism for this practically important ion dissociation.

Acknowledgements

Support of this research by the NIH-National Institute of Diabetes, Digestive and Kidney Diseases (grant no. R01 DK067859) and the National Science Foundation (grant no. CHE-1055132) is gratefully acknowledged. The Department of Chemistry Computational Center has been supported jointly by the National Science Foundation and the University of Washington.

REFERENCES

- [1] A. J. Pearson, W. R. Roush. *Handbook of Reagents for Organic Synthesis - Activating Agents and Protecting Groups*, John Wiley & Sons, **1999**, 83. http://www.knovel.com/web/portal/browse/display?_EXT_KNOVEL_DISPLAY_bookid=2129&VerticalID=0
- [2] I. W. Ashworth, B. G. Cox, B. Meyrick. Kinetics and mechanism of N-Boc cleavage: Evidence of a second-order dependence upon acid concentration. *J. Org. Chem.* **2010**, *75*, 8117–8125.
- [3] G. V. Garner, D. B. Gordon, L. W. Tetler, R. D. Sedgwick, Fast atom bombardment mass spectrometry of butyloxycarbonyl protected (BOC) amino acids. *Org. Mass Spectrom.* **1988**, *18*, 486–488.
- [4] M. H. Gelb, F. Tureček, C. R. Scott, N. A. Chamoles. Direct multiplex assay of enzymes in dried blood spots by tandem mass spectrometry for the newborn screening of lysosomal storage disorders. *J. Inher. Metab. Dis.* **2006**, *29*, 397–404.
- [5] F. Tureček, C. R. Scott, M. H. Gelb. Tandem mass spectrometry in the detection of inborn errors of metabolism for newborn screening. *Methods Mol. Biol.* **2007**, *359*, 143–157. (Quantitative Proteomics by Mass Spectrometry)
- [6] Y. Li, C. R. Scott, N. A. Chamoles, A. Ghavami, B. M. Pinto, F. Tureček, M. H. Gelb. Direct multiplex assay of lysosomal enzymes in dried blood spots for newborn screening. *Clin. Chem.* **2004**, *50*, 1785–1796.
- [7] T. A. Duffey, G. Bellamy, J. Diaker, S. Elliott, M. Glass, C. R. Scott, F. Tureček, M. H. Gelb, Triplex tandem mass spectrometry for newborn screening of Fabry, Pompe and mucopolysaccharidosis I (Hurler Syndrome): Results of a pilot study. *Clin. Chem.* **2010**, *56*, 1854–1861.
- [8] Z. Spáčil, S. Elliott, S. L. Reeber, M. H. Gelb, C. R. Scott, F. Tureček. Comparative fast liquid chromatography: Application to newborn screening of Pompe, Fabry, and Hurler diseases. *Anal. Chem.* **2011**, *84*, 4822–4828.
- [9] S. Blanchard, M. Sadílek, C. R. Scott, F. Tureček, M. H. Gelb. Tandem mass spectrometry for the direct assay of lysosomal enzymes in dried blood spots: Application to screening newborns for mucopolysaccharidosis I (Hurler-Scheie syndrome). *Clin. Chem.* **2008**, *54*, 2067–2070.
- [10] D. Wang, T. Wood, M. Sadílek, C. R. Scott, F. Tureček, M. H. Gelb. Tandem mass spectrometry for the direct assay of enzymes in dried blood spots: Application to newborn screening for mucopolysaccharidosis II (Hunter disease). *Clin. Chem.* **2007**, *53*, 137–140.
- [11] B. Wolfe, S. Blanchard, M. Sadílek, C. R. Scott, F. Tureček, M. H. Gelb. Tandem mass spectrometry for the direct assay of lysosomal enzymes in dried blood spots: Application to screening newborns for mucopolysaccharidosis II (Hunter syndrome). *Anal. Chem.* **2011**, *83*, 1152–1156.

- [12] T. Khaliq, M. Sadilek, C. R. Scott, F. Tureček, M. H. Gelb. Tandem mass spectrometry for the direct assay of lysosomal enzymes in dried blood spots: Application to screening newborns for mucopolysaccharidosis IVA (Morquio A). *Clin. Chem.* **2011**, *57*, 128–131.
- [13] T. A. Duffey, M. Sadilek, C. R. Scott, F. Tureček, M. H. Gelb. Tandem mass spectrometry for the direct assay of lysosomal enzymes in dried blood spots: Application to screening newborns for mucopolysaccharidosis VI (Maroteaux–Lamy syndrome). *Anal. Chem.* **2010**, *82*, 9587–9591.
- [14] M. Remko. Ab initio MO study of protonation of carbamic acid, methyl carbamate and methyl *N*-methylcarbamate. *Collect. Czech. Chem. Commun.* **1988**, *53*, 1141–1148.
- [15] J. A. Gregersen, C. Hao, F. Turecek. Electron super-rich radicals. III. On the peculiar behavior of the aminodihydroxymethyl radical in the gas phase. *J. Phys. Chem. A* **2009**, *113*, 5855–5864.
- [16] M. J. Frisch, G. W. Trucks, H. B. Schlegel, G. E. Scuseria, M. A. Robb, J. R. Cheeseman, G. Scalmani, V. Barone, B. Mennucci, G. A. Petersson, H. Nakatsuji, M. Caricato, X. Li, H. P. Hratchian, A. F. Izmaylov, J. Bloino, G. Zheng, J. L. Sonnenberg, M. Hada, M. Ehara, K. Toyota, R. Fukuda, J. Hasegawa, M. Ishida, T. Nakajima, Y. Honda, O. Kitao, H. Nakai, T. Vreven, J. A. Montgomery, Jr, J. E. Peralta, F. Ogliaro, M. Bearpark, J. J. Heyd, E. Brothers, K. N. Kudin, V. N. Staroverov, R. Kobayashi, J. Normand, K. Raghavachari, A. Rendell, J. C. Burant, S. S. Iyengar, J. Tomasi, M. Cossi, N. Rega, J. M. Millam, M. Klene, J. E. Knox, J. B. Cross, V. Bakken, C. Adamo, J. Jaramillo, R. Gomperts, R. E. Stratmann, O. Yazyev, A. J. Austin, R. Cammi, C. Pomelli, J. W. Ochterski, R. L. Martin, K. Morokuma, V. G. Zakrzewski, G. A. Voth, P. Salvador, J. J. Dannenberg, S. Dapprich, A. D. Daniels, O. Farkas, J. B. Foresman, J. V. Ortiz, J. Cioslowski, D. J. Fox. *Gaussian 09, Revision A.02*, Gaussian, Inc.: Wallingford CT, **2009**.
- [17] (a) A. D. Becke. New mixing of Hartree-Fock and local density-functional theories. *J. Chem. Phys.* **1993**, *98*, 1372–1377.
(b) A. D. Becke. Density functional thermochemistry. III. The role of exact exchange. *J. Chem. Phys.* **1993**, *98*, 5648–5652.
(c) P. J. Stephens, F. J. Devlin, C. F. Chabalowski, M. J. Frisch. Ab initio calculation of vibrational absorption and circular dichroism spectra using density functional force fields. *J. Phys. Chem.* **1994**, *98*, 11623–11627.
- [18] G. Rauhut, P. Pulay. Transferable scaling factors for density functional derived vibrational force fields. *J. Phys. Chem.* **1995**, *99*, 3093–3100.
- [19] C. Møller, M. S. Plesset. A note on an approximation treatment for many-electron systems. *Phys. Rev.* **1934**, *46*, 618–622.
- [20] F. Tureček. Proton affinity of dimethyl sulfoxide and relative stabilities of C₂H₆OS molecules and C₂H₇OS⁺ ions. A comparative G2 (MP2) ab initio and density functional theory study. *J. Phys. Chem. A* **1998**, *102*, 4703–4713.
- [21] J. Čížek, J. Paldus, L. Šroubková. Cluster expansion analysis for delocalized systems. *Int. J. Quant. Chem.* **1969**, *3*, 149–167.
- [22] G. D. Purvis, R. J. Bartlett. A full coupled-cluster singles and doubles model. The inclusion of disconnected triples. *J. Chem. Phys.* **1982**, *76*, 1910–1918.
- [23] L. A. Curtiss, K. Raghavachari, J. A. Pople. Gaussian-2 theory using reduced Møller-Plesset orders. *J. Chem. Phys.* **1993**, *98*, 1293–1298.
- [24] J. Tomasi, B. Mennucci, R. Cammi. Quantum mechanical continuum solvation models. *Chem. Rev.* **2005**, *105*, 2999–3093.
- [25] F. Tureček, C. J. Cramer. Thermochemistry of simple enols and enol cation-radicals revisited. A G2(MP2) ab initio study. *J. Am. Chem. Soc.* **1995**, *117*, 12243–12253.
- [26] R. G. Gilbert, S. C. Smith. *Theory of Unimolecular and Recombination Reactions*, Blackwell Scientific Publications: Oxford, **1990**, 52–132.
- [27] L. Zhu, W. L. Hase. *Quantum Chemistry Program Exchange*, Indiana University: Bloomington, **1994**. Program No. QCPE 644.
- [28] A. J. Frank, M. Sadilek, J. G. Ferrier, F. Tureček. Sulfur oxyacids and radicals in the gas phase. A variable-time neutralization-photoexcitation-reionization mass spectrometric and ab initio/RRKM study. *J. Am. Chem. Soc.* **1997**, *119*, 12343–12353.
- [29] W. A. Chupka. Effect of unimolecular decay kinetics on the interpretation of appearance potentials. *J. Chem. Phys.* **1959**, *30*, 191–211.
- [30] K. M. Ervin. Experimental techniques in gas-phase ion thermochemistry. *Chem. Rev.* **2001**, *101*, 391.